HHS Public Access

Author manuscript

Nat Nanotechnol. Author manuscript; available in PMC 2020 September 01.

Published in final edited form as:

Nat Nanotechnol. 2019 September ; 14(9): 858–865. doi:10.1038/s41565-019-0514-y.

Step-defect guided delivery of DNA to a graphene nanopore

Manish Shankla[†], **Aleksei Aksimentiev**[‡]

[†]Department of Physics, University of Illinois, 1110 W. Green St., Urbana, IL

[‡]Department of Physics, Beckman Institute for Advanced Science and Technology, University of Illinois, 1110 W. Green St., Urbana, IL

Abstract

Precision placement and transport of biomolecules are critical to many single molecule manipulation and detection methods. One such method is nanopore sequencing, where delivery of biomolecules toward a nanopore controls the method's throughput. Using all-atom molecular dynamics, here we show that precision transport of biomolecules can be realised by utilising ubiquitous features of a graphene surface-step defects that separate multilayer domains. Subject to an external force, we find adsorbed DNA to move much faster down a step defect than up, and even faster along the defect edge, regardless of whether the motion is produced by a mechanical force or a solvent flow. We utilise this direction dependency to demonstrate a mechanical analog of an electric diode and a system for delivering DNA molecules to a nanopore. The defect-guided delivery principle can be used for separation, concentration and storage of scarce biomolecular species, on-demand chemical reactions and nanopore sensing.

Precision transport of biomolecules is critical to any practical nanoscale workbench where biomolecules from unrefined samples are sorted, isolated, detected or identified in an automated, high-throughput manner. Current state-of-the-art nanofluidic systems already permit sorting[1,2] and separation[3] of biomolecules, multiplexing general purpose biochemical assays[4,5] and even integration with on-chip technologies for enhanced functionalities.[6,7] Nanopore sequencing[8] is one such emerging technology where delivery of biomolecules to a nanopore sequence sensor crucially affects the overall fidelity of the sequence determination.[9]

In a typical nanopore measurement, an electrically charged biomolecule is attracted toward a nanopore sensor by a gradient of the electric potential that extends from the nanopore opening into the surrounding electrolyte solution.[10] The presence of a biomolecule in a

Correspondence and requests for materials should be addressed to A. Aksimentiev. aksiment@illinois.edu.

Author contributions

A.A. conceived the project and carried out all AFM measurements. M.S. carried out all MD simulations and developed a theoretical model. AA and MS designed the computational experiments, analysed the data and co-wrote the manuscript.

Data availability statement

The data that support the plots within this paper and other findings of this study are available from the corresponding author upon reasonable request.

Additional Information

Supplementary information is available in the online version of the paper.

nanopore reduces the ionic current through the nanopore, which, in the case of DNA and RNA molecules, can report their nucleotide content[11,12] or even the nucleotide sequence of the molecules. [13] However, the outcome of a nanopore measurement strongly depends on the manner the biomolecule enters the nanopore. In particular, pore clogging, which can result from non-specific interactions between the biomolecule and the nanopore or uncontrolled secondary structure formation, affects both the throughput and precision of a nanopore measurement.[14-16]

While DNA and RNA sequencing is presently realised using biological nanopores,[17,18] nanopores in solid-state materials hold promise for further improvements of the nanopore sequencing method by offering a multi-modal DNA base readout,[19-23] mechanically robust membranes of indefinite shelf life, and massively scalable manufacturing strategies.[24] Among many possibilities, [25-27] graphene stands out as the most extensively studied[28-30] and versatile[31] material that can enable, in theory, nanopore measurements with angstrom precision because of its single-atom thickness. However, strong physisorption of DNA onto the graphene has so far severely limited sensing and sequencing applications of graphene nanopores.[14] Several methods have been applied to decrease the adsorption of DNA onto graphene, such as using electrolytes of high ion concentration and high pH[15] or coating graphene with amphiphilic molecules,[14] noticeably increasing the likelihood of double-stranded DNA translocation through a graphene nanopore. However, realising single-file transport of single-stranded DNA (ssDNA) or RNA molecules—the form of nucleic acids most amenable to nanopore sequencing—remains a major challenge, in particular for narrow (3 nm diameter or less) pores, which are best suited for sequencing applications.

Here, we theoretically demonstrate a system for capturing minute amounts of ssDNA and delivering them to an array of graphene nanopores in a highly regular, deterministic manner. Instead of fighting physisorption we embrace it to guide the transport of adsorbed ssDNA molecules along the edge of step defects, to and away from a graphene nanopore.

Direction dependence of forced displacement over a defect

Mechanical exfoliation of highly-oriented pyrolytic graphite (HOPG) produces terrace-like structures at the surface of the cleaved HOPG samples which can be imaged using atomic force microscopy (AFM).[32] Indeed, AFM images of a freshly cleaved HOPG surface—an imprint of the surface of a graphene membrane—reveal multiple micron-size regions of atomically flat carbon surfaces separated by step defects that vary in size from single to tens of carbon layers, Fig. 1a and Supplementary Fig. 1.

Using AFM in the tapping mode, we imaged DNA adsorbed to cleaved HOPG, finding that a moving tip of the AFM can displace DNA along the graphene surface, increasing DNA concentration at the step defects. Figure 1b shows a surface of cleaved HOPG after incubation with 0.1 ng/μl of M13 ssDNA, imaged in air. In addition to the familiar terrace-like features, the image reveals local filament-like structures that rise above the HOPG surface by approximately 2 nm, Supplementary Fig. 1, which we interpret as individual M13 molecules adsorbed onto the surface. The DNA placement at the surface is, however, not permanent and can be affected by the motion of the AFM tip despite being imaged in dry

(air) conditions, Supplementary Movies 1 and 2. Likely because of such displacements, the majority (82%) of the DNA molecules are found near the HOPG edges that occupy a small fraction (2.7%) of the total image area, Supplementary Fig. 2. Indeed, the direction of DNA displacement and DNA localisation along the HOPG edges was previously found to be consistent with the scanning directions of the AFM tip.[33,34]

AFM tip-induced displacements of ssDNA along an HOPG surface are even more profound when imaged in solution, Fig. 1c. In solution, the images of ssDNA adsorbed to graphene plateaus are much more smeared out in comparison to similar images obtained in air. The configuration of a DNA molecule at the graphene surface is seen to change appreciably between sequential scans of the same surface area, Fig. 1c. But even in solution, the DNA molecules are found to preferentially localise at, Supplementary Fig. 2, and move along, Supplementary Movie 3, the step defects.

MD simulations reveal that the force required to displace ssDNA over a step defect depends on the displacement direction. A typical simulation system, Fig. 2a, contained a rectangular patch of graphene slanted with respect to the one axis of the coordinate system to overlay the patch with itself under the periodic boundary conditions, producing an array of single step defects separated by the length of the periodic cell, Fig. 2b. After 40 ns of equilibration simulation, the DNA adsorbed to graphene with DNA bases forming hydrophobic contacts.[35,36] Constant velocity steered MD (cv-SMD) method was then used to displace the DNA molecule in one of the following three directions, Fig. 2b: perpendicular to and up the step (teal arrow), perpendicular to and down the step (orange arrow), and parallel to the step (purple arrow). Supplementary Movies 4-6 illustrate typical simulation trajectories.

As the DNA molecule is pulled multiple times up or down the step defects, the force increases sharply as the molecule approaches a defect and drops off rapidly after the molecule crosses the defect, Fig. 2c-e. The peak values of the force visibly depend on the pulling direction: pulling the DNA molecule up the step requires higher force than down the step regardless of the pulling speed. The average peak force required to move ssDNA up the step is 2 to 2.5 times larger than down the step, Fig. 2f, implying that displacement of ssDNA up the step encounters more resistance than down the step. In contrast, pulling the DNA molecule parallel to the step does not produce any discernible variation of the pulling force as the molecule does not cross any step defects. The average force applied to pull the DNA parallel to the step is an order of magnitude lower than that for pulling the molecule up or down the step regardless of the pulling speed, Fig. 2g. Note that the absolute values of the pulling force decrease with the pulling speed[37] and can be expected to match experimental values at experimental pulling speeds.

The logarithmic dependence of the average force on the DNA pulling velocity and the two-fold difference in the peak force for moving the DNA down and up a step defect, Fig. 2f, suggest that, subject to a force of a magnitude between the two average peak force values, the DNA molecule would be displaced predominantly down the step. We observed exactly that when the same ssDNA molecule was pushed in opposite directions by a constant force of 400 pN magnitude, Fig. 3a. Repeating the same simulations at a higher, 800 pN force produces an even more pronounced difference in ssDNA displacement, Fig. 3b and

Supplementary Fig. 3. At a smaller force of 200 pN, which is considerably lower than either up or down peak forces, the DNA displacement is confined to the region between the step defects. Orders of magnitude larger displacements of DNA are observed when the force is directed parallel to the step defect, Fig. 3b.

A practical way to produce lateral displacements of ssDNA along a patterned graphene surface is by the means of a hydrodynamic drag of a fluid flow that in turn can be produced by either a hydrostatic pressure gradient or an electro-osmotic flow.[3,7,38] We have reproduced such steady flow conditions in our MD simulations by imposing a pressure gradient in the slit-like geometry of our simulation system, Fig. 3c, see Methods for details. Unlike in a typical Poiseuille flow, the profile of flow velocity, V_{flow}, decreases asymmetrically from it's maximum near the centre of the slit towards the graphene membrane walls because of the presence of the step defects. We found the flow-induced displacement of ssDNA under a pressure gradient of the same magnitude to be smaller when the molecule moved up the step than when it moved down the step. Orders of magnitude faster ssDNA displacements were observed when the flow was directed parallel to the step defect, Fig. 3d.

The step defect-induced asymmetry of forced displacement was found to be robust with regard to chemical, Fig. 3e,f, and geometrical, Fig. 3f,h, features of the step defect. When pushed parallel to a curved defect line, adsorbed DNA followed the defect line without crossing, Supplementary Fig. 6.

Differential hydrophobic effect underlines the asymmetry

While moving a DNA molecule along a defectless surface of graphene can be expected to require less force then moving the same molecule with the same speed up or down the defect, the two-fold difference in the force required to move the DNA up or down a step defect is intriguing. To determine the physical mechanism that underlies such an asymmetry, we examined the force displacement of a single nucleotide up and down the step defect, Fig. 4a,b. In qualitative agreement with the behaviour observed for a longer DNA fragment, Fig. 2d, displacement of a single nucleotide up a step defect, Fig. 4c, requires a considerably higher peak force than displacement of the same nucleotide down the defect, Fig. 4d. The difference, however, is not only in the magnitude but also in the shape of the force–distance curves: a single, asymmetric force maximum is observed when the nucleotide is moved up the step but two shallower maxima are observed when moving the nucleotide in the opposite direction. The average excess work associated with pulling the nucleotide up and down the step is approximately 18 and 6 $k_{\text{B}}T$, Fig. 4e, in general agreement with the ~11.5 $k_{\text{B}}T$ dissociation energy of a pyrimidine nucleotide extracted from AFM measurements.[39]

As DNA adhesion to graphene is predominantly governed by hydrophobic forces [35,40], we examined hydration of the nucleotide as it is being pulled across the step, Fig. 4f,g. Moving against the step, the nucleotide dehydrates when encountering a step defect, before the pulling force starts to rise. The nucleotide rehydrates shortly after crossing the defect and after the force subsides. Moving down the step, the nucleotide first gains hydration as its side extends over the top surface of the step defect, which corresponds to the first increase of

the pulling force confirming an intuitive expectation that hydration is energetically unfavourable. The nucleotide loses hydration after adhering to the bottom layer of the defect as the pulling force drops and regains hydration away from the step defect, which produces a second increase of the pulling force.

Away from the defect, the nucleotide's hydration is the same and there is no energy bias for being at either side of the defect. One can also expect the directional dependence of the pulling force to disappear when the nucleotide is moved infinitely slow across the defect as the nucleotide can explore all states along the transition path with the same likelihood regardless of the pulling direction. However, a finite magnitude pulling force increases the probability of visiting the low hydration state when the nucleotide is pulled against the step defect, Fig. 4h. This kinetic effect produces the direction-dependence of the pulling force, which is similar to the action of a molecular ratchet.[41]

Unidirectional transport under oscillating force

The direction-dependence of forced ssDNA displacement across a step defect lends itself to design of systems for transportation, separation or concentration of adsorbed biomolecules. Previous experimental and computational studies have found the adhesion strength of DNA nucleotides to sensitively depend on the type of the DNA nucleotides.[39,40] Because the probability of a step-defect crossing event is governed by the adhesive forces, it may be possible to use such step defects to separate DNA molecules according to their nucleotide composition.

Figure 5a illustrates the state of the simulation system at the end of four consecutive 10 ns MD simulations. In each simulation, a pressure gradient was applied to produce solvent flow through the channel. The direction of the pressure gradient, and of the solvent flow, was reversed every 10 ns. At the end of the two cycles of the pressure gradient reversal, the DNA was displaced to the right from its initial location, down the step defect ladder. Figure 5b plots the CoM coordinate of the DNA fragment as a function of simulation time for three simulations carried out at several speeds of the alternating flow. In all simulations, the oscillating flow was found to produce directional motion of the adsorbed DNA molecule, although the magnitude of the displacement was found to depend on the flow magnitude, in accordance with our previous findings, Fig. 3d. Supplementary Movie 7 illustrates one such MD trajectory. Interestingly, displacements of a poly$(dA)_{20}$ strand subject to the same oscillating flow, Fig. 5b, was much less pronounced in comparison to that of poly$(dT)_{20}$, which is consistent with the stronger adsorption of adenine nucleotides to graphene.[39,40] Thus, a ladder of step defects can rectify an oscillating external force to produce unidirectional displacement of an adsorbed molecule down the step defect direction and separate DNA molecules according to their nucleotide composition.

DNA delivery to and away from a nanopore

The application of the mechanical rectification principle to a system of concentric terraces surrounding a nanopore, a feature frequently observed in graphene nanopore fabrication experiments, [42] does not bring an adsorbed DNA molecule toward the nanopore: the DNA

molecules move along the defect line around the nanopore to the opposite side of the terrace rather than sliding down the step toward the nanopore, Supplementary Movie 8-10.

We designed our nanopore delivery system to consist of two single layer-depth spiral patterns of opposite chirality connected by a nanopore at the centre of the two spirals, Fig. 6a. At the beginning of the DNA delivery simulation, a poly$(dT)_{20}$ strand is adsorbed to the top graphene sheet at the periphery of the simulation system, Fig. 6b. The molecule is then subject to a constant-magnitude force that changes its direction by 90 degrees in a clockwise manner while remaining parallel to the graphene membrane, Fig. 6c, while a constant 500 mV bias is applied across the graphene membrane. Subject to the external force, the molecule is seen to move along the spiral toward, through and away from the nanopore, Fig. 6b,d. Supplementary Movie 11 illustrates the simulation trajectory. Guided delivery of ssDNA to a graphene nanopore was realised in a simulation carried out under a lower magnitude force, Supplementary Movie 12, and when the DNA motion was produced by a fluid flow that changed its direction by 90 degrees in a clockwise manner, Supplementary Movie 13. We also used the alternating fluid flow protocol to deliver a peptide chain to the graphene nanopore, Supplementary Movie 14, which shows a potential utility of our approach for protein fingerprinting and sequencing.[43] Importantly, the force direction protocol applied unaltered for the whole duration of the simulation, meaning that DNA was guided toward, through and away from the nanopore in a ”blind” manner. Thus, a DNA molecule adsorbed anywhere on a graphene nanopore spiral will be delivered to the nanopore located at the centre of the spiral as long as the guiding force protocol has the same chirality as the spiral. The same force protocol will also remove the molecule away from the nanopore after the molecule completes nanopore translocation, preventing nanopore clogging.

Using a theoretical model (see Supplementary Note 1 and Supplementary Fig. 7), we estimated the performance of our nanopore delivery system at experimentally accessible magnitudes (0.5–5.0 μN) and switching times (1–100 μs) of the driving force protocol and the guiding structure dimensions, R_{spiral}, of up to 5.5 μm, Fig. 6e. According to the model, a molecule placed initially at the outer edge of a 5.5 μm radius structure will be captured by the nanopore in 3.2 ms subject to a guiding force of 1.0 pN changing its direction by 90 degrees every 90 μs in a 360 μs driving force cycle. The average time to capture decreases with the duration of the guiding force cycle but requires driving forces of higher magnitudes to ensure that the molecule travels a quarter of the segment along the spiral structure (90 degrees in the polar angle coordinate) before the driving force switches its direction.

As the guiding force protocol produces capture, translocation, and removal of adsorbed molecules regardless of their initial location within the guiding structure, the protocol can be applied to simultaneously capture many molecules in an array of nanopores, where each nanopore is equipped with a spiral guiding structure. Figure 6f plots the maximum theoretical throughput of such a nanopore array as a function of the linear dimension of the guiding nanopore structures. According to our estimate (detailed in Supplementary Note 1), a 1 mm^2 device containing 10^6 pores (R_{spiral} = 1 μm) will capture 10^8 ssDNA molecules per second for a 0.5 pN / 360 μs cycle guiding force protocol. Thus, the theoretical throughput of such a nanopore array is many orders of magnitude higher than the throughput of

commercial nanopore sequencing platform, minION (<100 molecules per second per device, see Supplementary Note 1 for details of the calculations). More importantly, because every molecule that lands on the structure is delivered for nanopore analysis, the nanopore array may remain operational even at ultra-low concentrations of DNA in the sample.

An experimental implementation of our DNA delivery system is well within reach of present day nanotechnology as the minimum lateral size of the nanostructures can exceed 10 nm. Furthermore, fabrication of a smoothly varying spiral structure, Fig. 6a, is not essential for realising step-defect delivery: a right-angled spiral can accomplish the same, Supplementary Movie 15. Furthermore, the spiral does not even have to be evenly etched: the only condition is that the depth must increase toward its centre, Supplementary Movie 16. Such spiral nanostructures can be fabricated by either growing the membrane layer-by-layer or by etching away layers of a multi-layer membrane stack, Supplementary Fig. 8. The lateral motion of DNA adsorbed to graphene can be realised by several methods, Supplementary Fig. 9, for example, by applying an electric field parallel to the membrane to induce electrophoretic[44] or electrokinetic[45] forces, a pressure-driven solvent flow[46] or even using a massively parallel AFM setup.[47] In the latter case, a synchronised motion of multiple AFM tips is not used to guide the molecules toward the pore, but only to ”scrub” the area occupied by the guiding structure, offering high throughput.

Conclusions

We have shown that step defects—ubiquitous features of graphene and other 2D materials—can be used to guide transport of adsorbed biomolecules. Such defect-guided transport of biomolecules can be of use in a diverse range of technological processes, from lab-on-chip sorting and synthesis of biomolecules to single molecule nanopore sequencing. Importantly, deliberate patterning of 2D materials with step defects is well within reach of modern nanofabrication technology, including electron beam patterning of nanometer features onto graphene by reducing DNA origami via carbonisation,[48] removal of single carbon atoms using a silicone adatom[49] or laser ablation.[50]

Methods

Atomic force microscopy

All AFM images were collected using the RIBM HS-AFM 1.0 instrument. The AFM measurements were performed in the tapping mode using Olympus AC 160 TS cantilevers; the resonant frequency and the spring constant of the cantilevers were 300 kHz and 42 N/m, respectively, and the tip’s radius was 9±2 nm. Measurements in solution were performed in a liquid flow cell. AFM images were processed using the plane subtraction and row alignment by a median of differences methods within the Gwyddion package.[51]

Prior to each measurement, all HOPG samples were freshly cleaved using the scotch tape method.[32] In the case of AFM imaging in air, a 1 μl droplet of buffer solution was placed on top of the HOPG sample. The sample was incubated for 10 minutes, rinsed with DI water and blowdried with nitrogen gas. For AFM imaging in solution, the buffer solution was introduced into the liquid flow cell; the flow cell was placed on top of the freshly cleaved

HOPG surface. The buffer solution containing 1 M KCl and 1 mM EDTA was prepared by mixing stock solutions of KCl and EDTA. The M13 DNA sample was first heated to 95 C, kept at that temperature for 20 minutes and then rapidly cooled on ice. The final sample was prepared by mixing DNA with the 1 KCl/1 mM EDTA buffer to achieve 0.1 ng/μl concentration of DNA.

MD simulations

All MD simulations were performed using the program NAMD2,[52] a 2 fs integration time step, 2-2-6 multiple time-stepping, CHARMM27 parameter set,[53] a 7–8 Å cutoff for van der Waals and short-range electrostatic forces, the particle mesh Ewald (PME) method for long-range electrostatics[54] computed over a 1.1 Å grid and periodic boundary conditions. Simulations in the NPT ensemble (constant number of particles N, pressure P, and temperature T) were performed using a Lowe-Andersen thermostat,[55] and Nosé-Hoover Langevin piston pressure control[56] set at 295 K and 1 atm, respectively. Simulations in the NVT ensemble (constant number of particles N, volume V and temperature T) employed a Lowe-Andersen thermostat.[55] Visualisation and analysis were performed using VMD.[57]

All models of graphene membranes were generated using the Inorganic Builder plugin of VMD. Carbon atoms of graphene were modelled as type CA atoms of the CHARMM27 force field. [35] The step defect systems were built starting from a multilayer hexagonal graphene unit cell 80 Å on side. A step defect was generated by removing carbon atoms located between the midsection and an outer edge of the topmost graphene layer. The remaining singly bonded carbon atoms on the step edge were removed leaving a zig-zag edge. The graphene sheets were tilted by 2.2 degrees (3.5 degrees for the double-layer defect system) with respect to the z-axis to form a continuous, infinite plane containing one step defect per unit cell under periodic boundary conditions.

Chemical modification of the step defect was performed by attaching a hydrogen atom or a carboxyl group to all double bonded carbon atoms located at the graphene edge. For the hydrogen passivated step defect, each hydrogen molecule carried a partial charge of $+0.16e$ (where e is the charge of a proton) and the carbon atom it was bonded to carried a partial charge of $-0.16e$.[58] The parameters for each carboxyl group were taken from the CHARMM27 force field model of a glutamic acid. The carboxylate groups each carried a net charge of -1 e.

A poly(dT)$_{20}$·poly(dA)$_{20}$ B-form DNA duplex was built using the 3D-DART webserver.[59] The poly(dA) strand was then removed and the remaining poly(dT)$_{20}$ strand was placed parallel to the graphene layer 13 Å away (CoM distance) from the top carbon sheet. Water and ions were added to produce a neutral system containing 1 M KCl. Following a 240-step minimisation, the system was equilibrated in the NPT ensemble for 40 ns. The equilibrated model of the ssDNA strand was used to build the single nucleotide, double layer and chemically modified step defect systems. Each of the final systems was a hexagonal prism 114 Å on a side and 80 Å in height and contained approximately 81,000 atoms. Hexagonal prism boundary conditions were applied within the $x-y$ plane in all MD simulations.

The graphene system containing spiral groves was created by removing atoms from a three-layer hexagonal prism of carbon atoms 18.3 nm on each side and arranged perpendicular to the z axis. Two offset spirals were defined by the following parametric equations: [$x_1 = 30\ e^{0.14t}\cos(t) - 9$, $y_1 = 30\ e^{0.14t}\sin(t) + 15$] and [$x_2 = 30\ e^{0.14t}\cos(t) - 9$ and $y_2 = 30\ e^{0.14t}\sin(t) + 15$], where parameter t varied from -0.3π to 3.9π and x and y coordinated had units of angstroms. Atoms of the first carbon (upper-most) layer whose x and y coordinates were between the two offset spirals were removed. The spiral on the lowest graphene layer was created as a mirror image of the spiral on the topmost layer. A 2.0 nm-diameter nanopore at the center of the spiral was created by removing atoms from all three layers. Any singly bonded carbon atoms were removed. An equilibrated model of an ssDNA strand was taken from the single-step system and placed in the outermost segment of the spiral, on-top of the second layer. Water and ions were added to produce a neutral system containing 1 M KCl. This system was minimized for 600-steps and equilibrated in the NPT ensemble for 15 ns. The final system contained 510,641 atoms and spanned ~6 nm along the z axis.

All simulations of forced ssDNA migration were performed in the NVT ensemble. Constant velocity SMD simulations were performed by attaching one end of a virtual harmonic spring to the CoM of the DNA fragment (excluding the hydrogen atoms) and displacing the other end of the spring with a constant velocity. The spring constant was 0.4 and 1 kcal mol^{-1} Å^{-1} for poly(dT)$_{20}$ and single nucleotide pulling simulations, respectively. The lag distance between the virtual particle and the CoM of the molecule—the extension of the harmonic string—reported on the instantaneous force applied to the molecule. In the constant force simulations, the force of prescribed magnitude and direction was applied to the CoM of the DNA fragment (excluding hydrogen atoms). In the simulations of water flow-driven ssDNA migration, the pressure difference across the simulation cell was produced by applying a constant force, f_p, to all water molecules in the target direction of the water flow. The resulting pressure gradient $\Delta P = nf_p/A$, where n and A are the number of water molecules and the cross section of the $x - z$ plane of the period unit cell, respectively.

Supplementary Material

Refer to Web version on PubMed Central for supplementary material.

Acknowledgment

Research reported in this publication was supported by the National Human Genome Research Institute of the National Institutes of Health under award no. R01-HG007406, National Science Foundation under award no. DMR-0955959 and through a cooperative research agreement with Oxford Nanopore Technologies. The authors gladly acknowledge supercomputer time provided through XSEDE Allocation Grant MCA05S028 and the Blue Waters petascale supercomputer system at the University of Illinois at Urbana–Champaign. A.A. thanks Greg Schneider, Allard Katan and Cees Dekker for their help with setting up AFM measurements, the Department of Bionanosciences at the Delft University of Technology for hospitality and the Netherlands Organization for Scientific Research (NWO) for financial support.

References

(1). Han J & Craighead HG Separation of long DNA molecules in a microfabricated entropic trap array. Science 288, 1026–1029 (2000). [PubMed: 10807568]

(2). Huang LR, Cox EC, Austin RH & Sturm JC Continuous particle separation through deterministic lateral displacement. Science 304, 987–990 (2004). [PubMed: 15143275]

(3). Fu J, Schoch RB, Stevens AL, Tannenbaum SR & Han J A patterned anisotropic nanofluidic sieving structure for continuous-flow separation of DNA and proteins. Nat. Nanotech 2, 121–128 (2007).

(4). Hong JW, Studer V, Hang G, Anderson WF & Quake SR A nanoliter-scale nucleic acid processor with parallel architecture. Nat. Biotech 22, 435 (2004).

(5). Sarkar A, Kolitz S, Lauffenburger DA & Han J Microfluidic probe for single-cell analysis in adherent tissue culture. Nat. Commun 5, 3421 (2014). [PubMed: 24594667]

(6). Fan X & White IM Optofluidic microsystems for chemical and biological analysis. Nat. Phot 5, 591 (2011).

(7). Wang C et al. Wafer-scale integration of sacrificial nanofluidic chips for detecting and manipulating single DNA molecules. Nat. Commun 8, 14243 (2017). [PubMed: 28112157]

(8). Branton D et al. The potential and challenges of nanopore sequencing. Nat. Biotech 26, 1146–1153 (2008).

(9). Wanunu M, Morrison W, Rabin Y, Grosberg AY & Meller A Electrostatic focusing of unlabelled DNA into nanoscale pores using a salt gradient. Nat. Nanotech 5, 169–165 (2010).

(10). Kasianowicz JJ, Brandin E, Branton D & Deamer DW Characterization of individual polynucleotide molecules using a membrane channel. Proc. Natl. Acad. Sci. U. S. A 93, 13770–13773 (1996). [PubMed: 8943010]

(11). Akeson M, Branton D, Kasianowicz JJ, Brandin E & Deamer DW Microsecond time-scale discrimination among polycytidylic acid, polyadenylic acid, and polyuridylic acid as homopolymers or as segments within single RNA molecules. Biophys. J 77, 3227–3233 (1999). [PubMed: 10585944]

(12). Meller A, Nivon L, Brandin E, Golovchenko J & Branton D Rapid nanopore discrimination between single polynucleotide molecules. Proc. Natl. Acad. Sci. U. S. A 97, 1079–1084 (2000). [PubMed: 10655487]

(13). Manrao EA et al. Reading DNA at single-nucleotide resolution with a mutant MspA nanopore and phi29 DNA polymerase. Nat. Biotech 30, 349–353 (2012).

(14). Schneider GF et al. Tailoring the hydrophobicity of graphene for its use as nanopores for DNA translocation. Nat. Commun 4, 3619 (2013).

(15). Garaj S, Liu S, Golovchenko JA & Branton D Molecule-hugging graphene nanopores. Proc. Natl. Acad. Sci. U. S. A 110, 12192–12196 (2013). [PubMed: 23836648]

(16). Shan YP et al. Surface modification of graphene nanopores for protein translocation. Nanotech. 24, 495102 (2013).

(17). Laszlo AH et al. Decoding long nanopore sequencing reads of natural DNA. Nat. Biotech 32, 829–833 (2014).

(18). Jain M et al. Improved data analysis for the MinION nanopore sequencer. Nat. Methods 12, 351–356 (2015). [PubMed: 25686389]

(19). Lagerqvist J, Zwolak M & Di Ventra M Fast DNA sequencing via transverse electronic transport. Nano Lett. 6, 779–782 (2006). [PubMed: 16608283]

(20). Gracheva ME et al. Simulation of the electric response of DNA translocation through a semiconductor nanopore-capacitor. Nanotech. 17, 622–633 (2006).

(21). Postma HWC Rapid sequencing of individual DNA molecules in graphene nanogaps. Nano Lett. 10, 420–425 (2010). [PubMed: 20044842]

(22). Huang S et al. Identifying single bases in a DNA oligomer with electron tunnelling. Nat. Nanotech 5, 868–873 (2010).

(23). Saha K, Drndić M & Nikolić BK DNA base-specific modulation of microampere transverse edge currents through a metallic graphene nanoribbon with a nanopore. Nano Lett. 12, 50–55 (2012). [PubMed: 22141739]

(24). Kim MJ, Wanunu M, Bell DC & Meller A Rapid fabrication of uniform size nanopores and nanopore arrays for parallel DNA analysis. Adv. Mater 18, 3149–3153 (2006).

(25). Dekker C Solid-state nanopores. Nat. Nanotech 2, 209–215 (2007).

(26). Liu K, Feng J, Kis A & Radenovic A Atomically thin molybdenum disulfide nanopores with high sensitivity for DNA translocation. ACS Nano 8, 2504–2511 (2014). [PubMed: 24547924]

(27). Zhou Z et al. Dna translocation through hydrophilic nanopore in hexagonal boron nitride. Sci. Reports 3, 3287 (2013).

(28). Garaj S et al. Graphene as a subnanometre trans-electrode membrane. Nature 467, 190–193 (2010). [PubMed: 20720538]

(29). Merchant CA et al. DNA translocation through graphene nanopores. Nano Lett. 10, 2915–2921 (2010). [PubMed: 20698604]

(30). Schneider GF et al. DNA translocation through graphene nanopores. Nano Lett. 10, 3163–3167 (2010). [PubMed: 20608744]

(31). Traversi F et al. Detecting the translocation of DNA through a nanopore using graphene nanoribbons. Nat. Nanotech 8, 939–945 (2013).

(32). Novoselov KS et al. Electric field effect in atomically thin carbon films. Science 306, 666 (2004). [PubMed: 15499015]

(33). Brett AMO & Paquim A-MC DNA imaged on a HOPG electrode surface by AFM with controlled potential. Bioelectrochemistry 66, 117–24 (2005). [PubMed: 15833711]

(34). Adamcik J, Klinov DV, Witz G, Sekatskii SK & Dietler G Observation of single-stranded dna on mica and highly oriented pyrolytic graphite by atomic force microscopy. FEBS Lett. 580, 5671–5675 (2006). [PubMed: 17007844]

(35). Wells DB, Belkin M, Comer J & Aksimentiev A Assessing graphene nanopores for sequencing DNA. Nano Lett. 12, 4117–4123 (2012). [PubMed: 22780094]

(36). Kim HS, Farmer BL & Yingling YG Effect of graphene oxidation rate on adsorption of poly-thymine single stranded DNA. Adv. Mater. Interfaces 4, 1601168 (2017).

(37). Evans E & Ritchie K Dynamic strength of molecular adhesion bonds. Biophys. J 72, 1541–1555 (1997). [PubMed: 9083660]

(38). Wang C et al. Hydrodynamics of diamond-shaped gradient nanopillar arrays for effective dna translocation into nanochannels. ACS Nano 9, 1206–1218 (2015). [PubMed: 25626162]

(39). Manohar S et al. Peeling single-stranded DNA from graphite surface to determine oligonucleotide binding energy by force spectroscopy. Nano Lett. 8, 4365–4372 (2008). [PubMed: 19368004]

(40). Lee J-H, Choi Y-K, Kim H-J, Scheicher RH & Cho J-H Physisorption of DNA Nucleobases on h-BN and Graphene: vdW-Corrected DFT Calculations. J. Phys. Chem C 117, 13435–13441 (2013).

(41). Astumian RD Thermodynamics and kinetics of a brownian motor. Science 276, 917–922 (1997). [PubMed: 9139648]

(42). Freedman KJ, Ahn CW & Kim MJ Detection of long and short DNA using nanopores with graphitic polyhedral edges. ACS Nano 7, 5008–5016 (2013). [PubMed: 23713602]

(43). Wilson J, Sloman L, He Z & Aksimentiev A Graphene nanopores for protein sequencing. Adv. Funct. Mater 26, 4830–4838 (2016). [PubMed: 27746710]

(44). Viovy JL Electrophoresis of DNA and other polyelectrolytes: Physical mechanisms. Rev. Mod. Phys 72, 813 (2000).

(45). Stein D, van der Heyden FH, Koopmans WJ & Dekker C Pressure-driven transport of confined dna polymers in fluidic channels. Proc. Natl. Acad. Sci. U. S. A 103, 15853–15858 (2006). [PubMed: 17047033]

(46). Squires TM & Quake SR Microfluidics: Fluid physics at the nanoliter scale. Rev. Mod. Phys 77, 977 (2005).

(47). Salaita K et al. Massively parallel dip–pen nanolithography with 55 000-pen two-dimensional arrays. Angew. Chem. Int. Ed 118, 7378–7381 (2006).

(48). Jin Z et al. Metallized DNA nanolithography for encoding and transferring spatial information for graphene patterning. Nat. Commun 4, 1663 (2013). [PubMed: 23575667]

(49). Russo CJ & Golovchenko JA Atom-by-atom nucleation and growth of graphene nanopores. Proc. Natl. Acad. Sci. U. S. A 109, 5953–7 (2012). [PubMed: 22492975]

(50). Sahin R, Simsek E & Akturk S Nanoscale patterning of graphene through femtosecond laser ablation. Appl. Phys. Lett 104, 053118 (2014).

(51). Nečas D & Klapetek P Gwyddion: an open-source software for SPM data analysis. Open Physics 10 (2012).

(52). Phillips JC et al. Scalable molecular dynamics with NAMD. J. Comput. Chem. 26, 1781–1802 (2005). [PubMed: 16222654]

(53). MacKerell Jr., A. D. Empirical force fields for biological macromolecules: Overview and issues. J. Comput. Chem 25, 1584–1604 (2004). [PubMed: 15264253]

(54). Darden TA, York D & Pedersen L Particle mesh ewald: An N log(N) method for ewald sums in large systems. J. Chem. Phys 98, 10089–92 (1993).

(55). Koopman EA & Lowe CP Advantages of a Lowe-Andersen thermostat in molecular dynamics simulations. J. Chem. Phys 124, 204103 (2006). [PubMed: 16774315]

(56). Martyna GJ, Tobias DJ & Klein ML Constant pressure molecular dynamics algorithms. J. Chem. Phys 101, 4177–4189 (1994).

(57). Humphrey W, Dalke A & Schulten K VMD: Visual molecular dynamics. J. Mol. Graphics 14, 33–38 (1996).

(58). He Y et al. Enhanced DNA sequencing performance through edge-hydrogenation of graphene electrodes. Adv. Funct. Mater 21, 2674–2679 (2011).

(59). van Dijk M & Bonvin AMJJ 3D-DART: A DNA structure modelling server. Nucleic Acids Res. 37, W235–W239 (2009). [PubMed: 19417072]

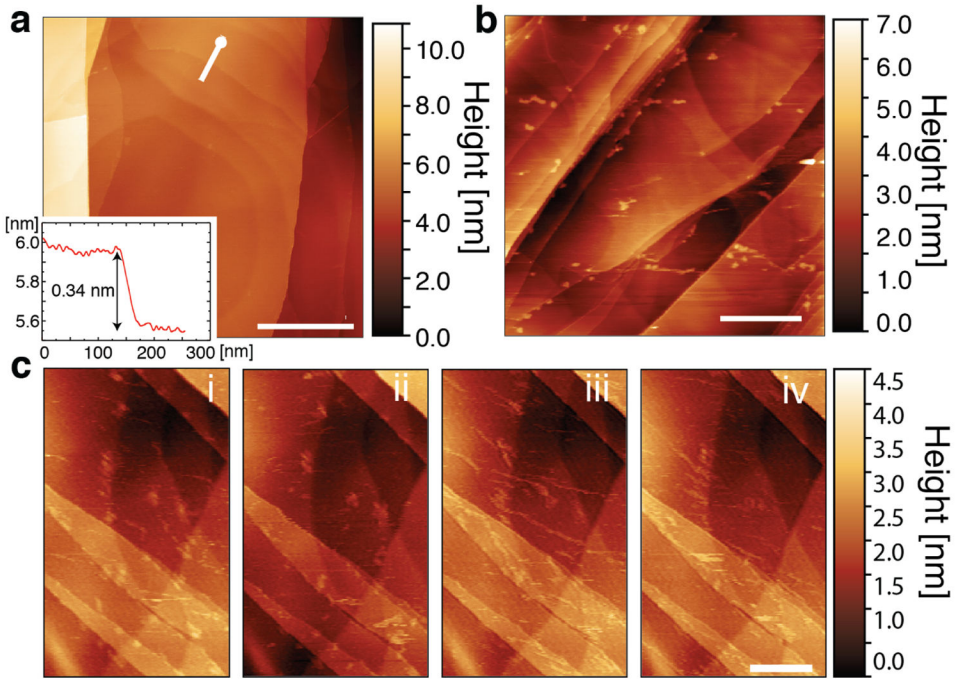

Figure 1:

DNA displacement and aggregation at defects along the surface of highly oriented pyrolytic graphite (HOPG) imaged using AFM. (a) AFM image of a typical mechanically exfoliated (scotch-tape method) HOPG sample in solution. The white line shows the height profile (inset graph) across a step defect on the HOPG sample. The circle on the line indicates 0 nm on the *x* axis in the inset graph. (b) AFM image of an HOPG sample incubated with 0.1 ng/μl of M13 ssDNA (see Methods) imaged in air. Single-stranded DNA aggregate along the edges of the step defects. The scale bars in panels a and b correspond to 500 nm. (c) Four sequential AFM images, denoted i to iv, of an HOPG sample incubated with 0.1 ng/μl of M13 ssDNA in solution. The scale bar correspond to 200 nm.

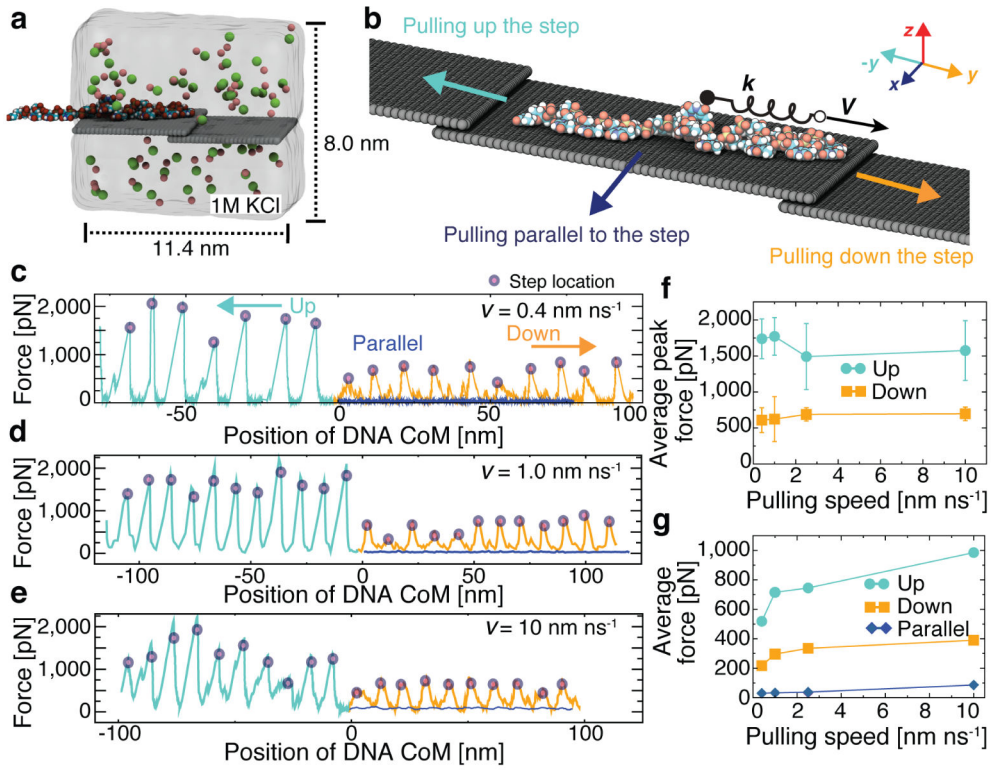

Figure 2:

Forced migration of a DNA strand over a step defect. (a) All-atom model of a graphene membrane containing a single step defect in a periodic unit cell, a poly(dT)$_{20}$ DNA strand, water and ions. The semi-transparent surface shows the volume occupied by water in a unit simulation cell. Carbon, nitrogen, oxygen and hydrogen atoms of DNA are shown as green, blue, red and white van der Waals spheres, respectively, carbon atoms of graphene are shown in grey. A small fraction of potassium and chloride ions are shown as green and pink spheres, respectively. (b) Schematics of the forced migration simulation. The centre-of-mass (CoM) of ssDNA is pulled down (+y), up (−y) and parallel to (+x) the step defect with a constant velocity v using a harmonic spring; extension of the spring reports on the applied force. Periodic images of the graphene membrane are shown in the −y and +y directions but omitted in the ±x directions for clarity. (c–e) The pulling force versus the CoM displacement of ssDNA. In each panel, orange, turquoise and blue lines indicate pulling down, up and parallel to the step defect, respectively. The purple-magenta dot represents the position at which the ssDNA molecules' CoM encounters the step defect. (f,g) The average peak force (f) and the average pulling force (g) versus the pulling speed for the three pulling directions. Error bars represent the standard deviation of mean computed treating maximum and average forces from each step crossing as independent measurements.

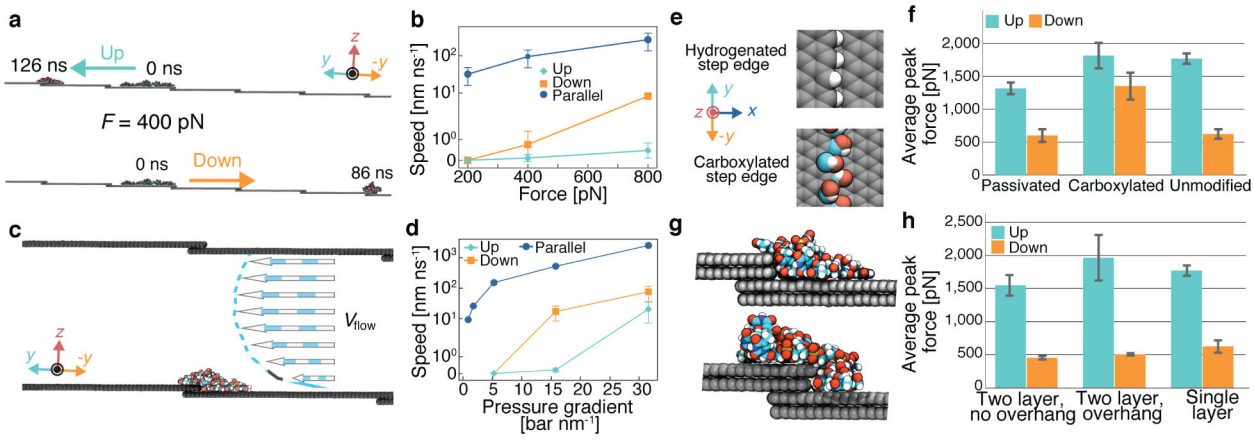

Figure 3:

Robustness of the step defect-induced asymmetry of forced displacement. (a) Constant force pulling of ssDNA across a step defect. A 20-nt ssDNA molecule is shown at the beginning and at the end of two simulations where the DNA was subject to the same magnitude constant force directed up (top) and down (bottom) the step defect (same as in Fig. 2b). Multiple periodic images of the unit cell are shown. (b) The average speed of ssDNA versus the magnitude of the constant force in the simulations where the constant force was directed up (cyan), down (orange) and parallel to (blue) the step defect. For each condition, the average velocity was computed by splitting five independent, 100 ns simulations into 5 ns fragments, beginning at the ssDNA's first encounter with the step defect, finding the average velocity for each fragment and averaging over the fragments. (c) Schematic illustration of the simulation setup where a directional flow of water (blue-white arrows) is produced via a hydrostatic pressure difference. The water velocity profile, V_{flow}, is shown as dashed lines and arrows. (d) The average speed of ssDNA versus the hydrostatic pressure gradient in the simulations where the pressure gradient was directed up (cyan), down (orange) and parallel to (blue) the step defect. Note the logarithmic scale of the vertical axes in panels b and d. (e) Schematic representation of two graphene edge terminations: passivation with hydrogen (top) and carboxylation (bottom). (f) The average peak pulling force required to cross hydrogen passivated, carboxylated and pure carbon step defects in cv-SMD simulations. (g) Double layer step defects containing no (top) or a single atom (bottom) overhang. Also shown is a typical configuration of ssDNA overcoming the defects. (h) The average peak pulling force required to cross the double layer step defects in cv-SMD simulations. Supplementary Figs. 3-5 show the simulation traces summarised in this figure. Error bars represent the standard deviation from the mean.

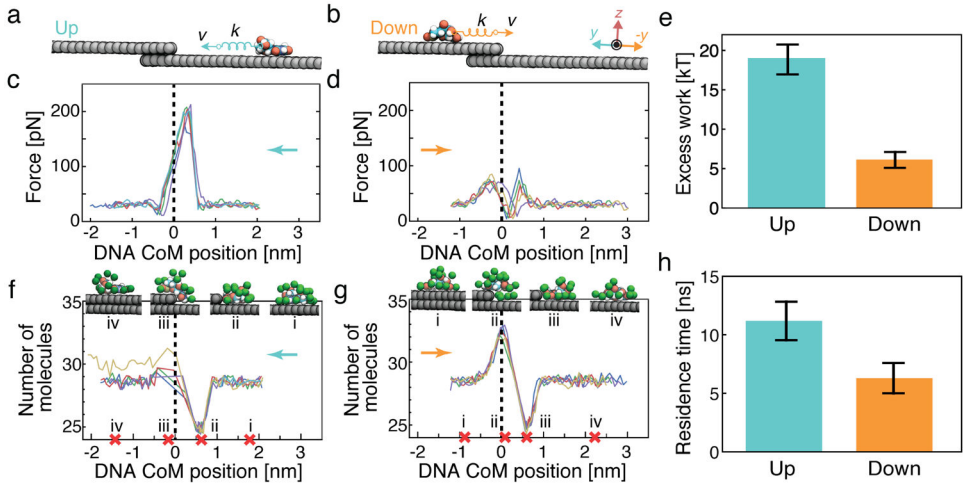

Figure 4:

Hydrophobic origin of the direction dependence of a defect crossing. (a,b) SMD simulation of a single nucleotide crossing a step defect. The CoM of a single nucleotide is pulled with a constant velocity of 0.1 nm ns^{-1} up or down a step defect. (c,d) Force applied to the DNA nucleotide by the SMD spring as a function of the nucleotide's CoM coordinate in five independent SMD simulations. The instantaneous SMD forces were averaged according to the CoM coordinate in 0.1 nm bins. The step defect is located at the origin and is schematically indicated by a vertical dashed line. The arrow indicates the direction of the forced displacement. (e) Average excess work done when moving a nucleotide across a step defect. The work was determined by integration of the force–displacement curves. The excess work was computed as the total work done on the nucleotide by the SMD force in the [−1.0, +1.0] nm interval minus the work done when moving the nucleotide equivalent distance along a flat graphene surface. (f,g) Number of water molecules surrounding the nucleotide as function of nucleotide location. The number was computed using a 0.4 nm cutoff and averaged according to the CoM coordinate in 0.1 nm bins. The snapshots illustrate representative configurations of water molecules (green van der Waals spheres) corresponding to the nucleotide's CoM coordinates marked by red crosses at the CoM axis. (h) Nucleotide residence time in the vicinity of the dehydration minimum defined as the [0.4, 0.8] nm interval along the CoM coordinate. Error bars represent standard deviations over five independent runs.

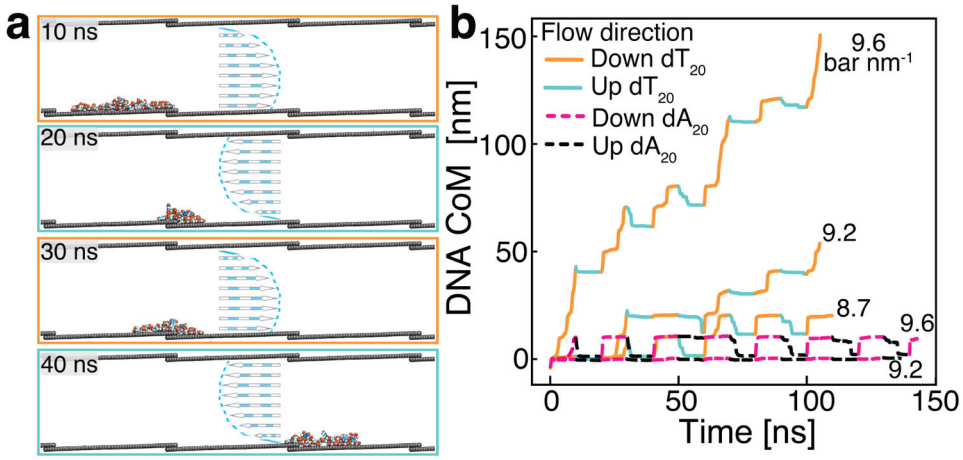

Figure 5:

Rectification of DNA displacement on a step-defect ladder. (a) Snapshots of a simulation system (same as in Fig. 3c) during an MD simulation in which the direction of the pressure gradient along the nanochannel was reversed every 10 ns. The pressure gradient magnitude was 9.2 bar nm^{-1}. In each snapshot, the water flow direction and magnitude are represented by the arrows. (b) CoM coordinate of a $poly(dT)_{20}$ (solid lines) and $poly(dA)_{20}$ (dashed lines) during MD simulations carried out under pressure gradient of the specified magnitude alternating direction every 10 ns. The colour of the line segments indicate DNA displacements corresponding to solvent flow directed up or down the step defects.

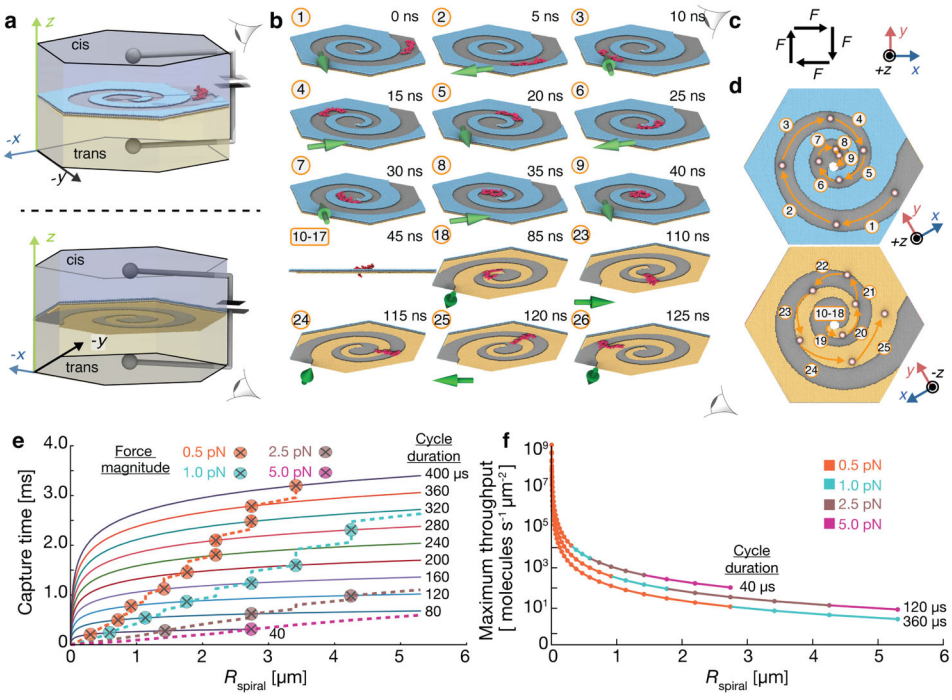

Figure 6:

Guided delivery of ssDNA to a graphene nanopore. (a) All-atom model of a guiding spiral structure viewed from the cis (top) and trans (bottom) compartments. The membrane consists of three stacked graphene layers. Single atom-depth spiral patterns are cutout from the top (blue) and bottom (yellow) sheets; a 2.0 nm-diameter nanopore is located at the centre of the spiral. The system is submerged in 1 M KCl solution (not shown); a transmembrane bias of 500 mV is applied across the membrane. At the beginning of a simulation, a molecule of ssDNA (red) is located at the outermost segment of the spiral. (b) Snapshots illustrating a 130 ns MD simulation of guided ssDNA transport. The direction of a 300 pN-magnitude force (green arrows) was changed by 90 degrees every 5 ns in a clockwise manner, which pushed ssDNA toward the nanopore along the cis side of the membrane and then away from the nanopore along the trans side. Some constant force fragments are omitted for clarity. (c) Schematic representation of the guiding force cycle. (d) Top-down (top) and bottom-up (bottom) views of the ssDNA's CoM path for the MD simulation illustrated in panel b. In panels b and d, the numbers specify the constant force fragments of the simulation. The force direction was changed 26 times within the 130 ns trajectory. (e) Average time required to capture a molecule as a function of the guiding structure's outer radius, R_{spiral}. For each cycle duration, a cross symbol indicates the maximum R_{spiral} value that permits deterministic nanopore capture at the specified force magnitude. (f) Maximum theoretical throughput of a nanopore array as a function of R_{spiral} and the force cycle duration. For each magnitude of the driving force (depicted in colour), the data terminate at a maximum radius that permits deterministic nanopore capture.